A major purpose of the Technical Information Center is to provide the broadest dissemination possible of information contained in DOE's Research and Development Reports to business, industry, the academic community, and federal, state and local governments.

Although a small portion of this report is not reproducible, it is being made available to expedite the availability of information on the research discussed herein.

LA-UR -85-513

CONF-850310--18

Los Alamos National Laboratory is operated by the University of California for the United States Department of Energy under contract W-7405-ENG-36

LA-UR--85-513

DE85 007709

TITLE STEADY-STATE SPHEROMAK REACTOR STUDIES

AUTHOR(S) R. A. Krakowski, Los Alamos National Laboratory, Los Alamos, NM
R. L. Hagenson, Phillips Petroleum Company, Bartlesville, OK

SUBMITTED TO Sixth ANS Topical Meeting on the Technology of Fusion Energy
San Francisco, California
March 3-7, 1985

DISCLAIMER

MASTER

Los Alamos National Laboratory
Los Alamos, New Mexico 87545

STEADY-STATE SPHEROMAK REACTOR STUDIES*

R. L. Hagenson** and R. A. Krakowski
Los Alamos National Laboratory
Los Alamos, New Mexico 87545
(505)667-5863

ABSTRACT
After summarizing the essential elements of a gun-sustained spheromak, the potential for a steady-state is explored by means of a comprehensive physics/engineering/costing model. A range of cost-optimized reactor design points is presented, and the sensitivity of cost to key physics, engineering, and operational variables is reported.

I. INTRODUCTION

Based on comprehensive parametric systems studies, strong developmental, operational, and economic arguments can be made[1] for improved fusion reactors with higher fusion-power-core (FPC, plasma chamber, first-wall, blanket, shield, coils) power density (MWt/m^3) or lower mass utilization (tonne/MWt). Studies of the compact, higher-power-density options[1] are extended here to include the spheromak member of the family of compact toroids (CT). After describing in Sec. II. the spheromak characteristics used to define the reactor, Sec. III. summarizes key elements of the engineering parametric model. Parametric results and sample design points for a range of net electric powers, P_E(MWe), and cost-of-electricity (COE) sensitivities to a range of physics, engineering, and operational/cost variables are given in Sec. IV. Section V. concludes with a brief physics and technology assessment.

II. BACKGROUND

A CT is an axisymmetric torus that has no magnet coils, conducting walls, or vacuum surfaces linking the torus. This configuration has poloidal field, B_θ, but may or may not support toroidal field, B_ϕ. The spheromak is a CT with both B_θ and B_ϕ fields, and both are of comparable magnitude within the plasma. The study of CTs is motivated by the potential for an improved reactor related to a simpler geometry and more efficient plasma confinement (higher beta).

The reactor potential of the spheromak is examined by comprehensive parametric analyses developed and refined for another related system.[1] Before this analysis can proceed, however, the means by which the spheromak is formed and sustained must be specified. Spheromaks have been generated using magnetized coaxial plasma guns (CTX[2], BETA-II[3]), combined fast-pulsed Z- and θ-pinch techniques (PS-1),[4] and electrodeless flux-core formation techniques (S-1).[5] Reactor projections have been made for spheromaks using the flux-core approach.[6] Extensions of the fast-pinch techniques to the reactor have not yet been envisaged. A range of other spheromak reactor studies based primarily on translating spheromaks that have been formed either by coaxial guns or flux-cores have also been reported.[6-9] The use of coaxial plasma-gun formation and sustainment of a stationary, steady-state spheromak reactor is investigated herein.

Figure 1. depicts the low-aspect-ratio spheromak and the formation/sustainment technique using the magnetized coaxial gun.[10] Application of a voltage between the gun electrodes produces a radial plasma current. This current generates a magnetic field that encircles the inner electrode and ultimately contributes to or amplifies the B_ϕ in the spheromak. The radial current interacts with this field to accelerate the highly conductive plasma towards the gun muzzle. Steady-state solenoids are depicted in Fig. 1 as embedded in the coaxial electrodes; these solenoids generate a magnetic field that diverges into a radial field at the gun muzzle. In a simplified view, this field is stretched by the accelerated plasma, forming the B_θ field after tearing, reconnection, and reformation into the spheromak configuration, which ultimately resides in an oblate metallic flux conserver. The actual process whereby flux from the gun is converted to flux in the spheromak is non-conservative and not fully understood.

Depending on operating mode,[10] the poloidal flux can be completely separated from the gun (separated spheromak), or a small fraction of the poloidal flux can remain attached to the gun electrodes (sustained

*Work performed under the auspices of the US Department of Energy, Office of Fusion Energy
**Phillips Petroleum Company, Bartlesville, OK 74004

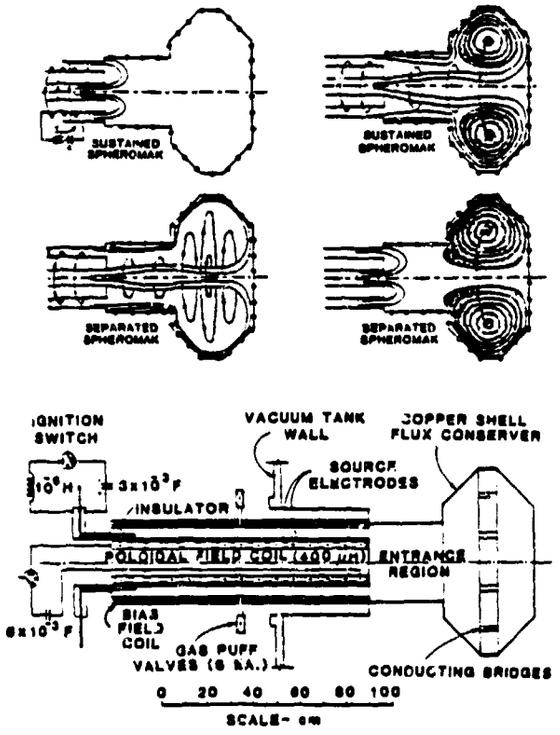

Fig. 1. Diagram of CTX spheromak facility.[2]

spheromak). The gross behavior and magnetic field profiles observed in either case are in agreement with Taylor's minimum-energy principle,[12] which describes the reversed-field pinch (RFP)[1] and simply states that a (zero-beta) plasma/field configuration injected into a conducting shell will relax to a near-minimum-energy configuration subject to the constraint of constant magnetic helicity, $K = \int \vec{A}\cdot\vec{B}dV_p$, with $\vec{B} = \nabla\times\vec{A}$. Magnetic helicity is a measure of flux linkage and is decreased by resistive decay of plasma currents. The case of the sustained spheromak (Fig. 1.) shows linked B_ϕ and B_θ entering the spheromak. If the rate of injection equals the rate of helicity consumption within the plasma, a means of steady-state sustainment is provided. The electrodes must be properly configured to allow the toroidal flux emerging from the gun, ϕ, ($\dot{\phi} = V_g$, where V_g is the gun voltage) to link that fraction ε of the total poloidal flux ψ that is open and connects with the gun.[11] The rate of helicity injection then is $2V_g\varepsilon\phi$, and must equal the rate of helicity decay. Experimental evidence for sustained spheromaks has been reported[10,13] for over 5 ms or ten times the magnetic-energy decay time, τ_B.[2]

These ideas and supporting experimental evidence serve as the basis of the spheromak reactor scoping study. The gun-electrode and flux-conserver geometry depicted in Fig. 1. is retained and scaled in Fig. 2. for the basic reactor model. The advantages of this fusion approach include:

- simply connected FPC
- potential for high plasma power density
- high level of intrinsic ohmic heating
- dc sustainment of magnetic fields
- stationary plasma operation
- possible to add natural magnetic separatrix and combine divertor function with gun-electrode system
- high engineering beta (plasma pressure normalized to magnetic field at coils)
  - low-field, low-current coils
  - efficient resistive coils
  - thin blanket/shield, high FPC power density, reduced FPC mass utilization, small systems, factory fabrication, etc.

The key disadvantages or uncertainties reside within the electrode system and the potential for impurity influx to the plasma.

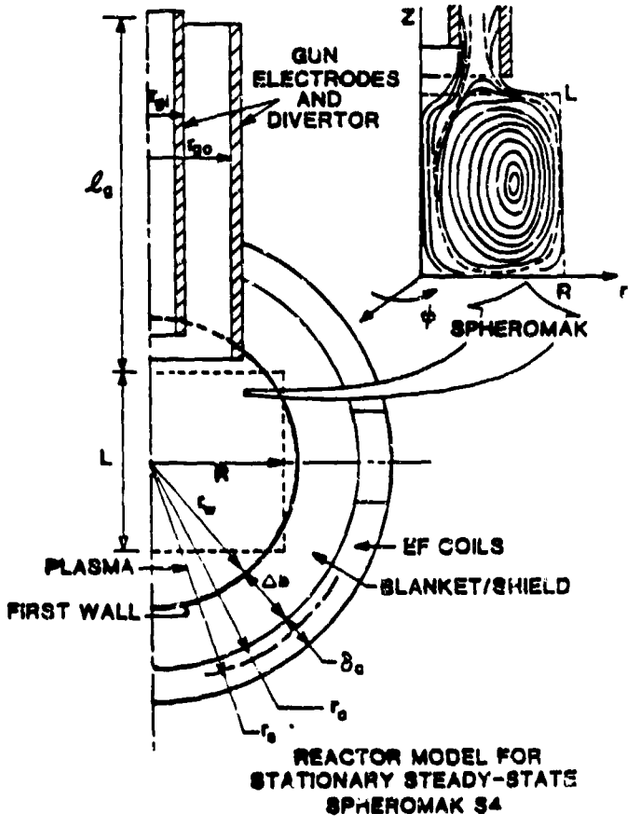

Fig. 2. Sustained-spheromak reactor model extrapolated from Fig. 1.

III. SPHEROMAK REACTOR MODEL

A. Parametric Systems Model

Figure 2 depicts a cylindrical equilibrium[14] model for the spheromak plasma which both conveniently and accurately provides plasma profile functions to the parametric systems model. The parametrics model is displayed in Fig. 3. and closely couples

performing a complete survey of steady-state reactor designs using COE as the object function. The desired net electric power, P_E, and the plasmoid oblateness, L/R, are specified. The equilibrium model provides flux functions that are used along with temperature and density profiles to generate a range of profile factors, g_i, needed to compute pressure balance, field levels, energy losses, and reaction rates. The outside plasma separatrix radius, R, is then varied for a given L/R. A range of equilibrium-field-coil (EFC) thicknesses is then surveyed, and the cost of coil conductor is traded against the electrical power recirculated to the resistive EFCs. At each coil thickness the ratio of coil current to toroidal plasma current is determined by locating the equilibrium separatrix position at the appropriate midplane radius, R.

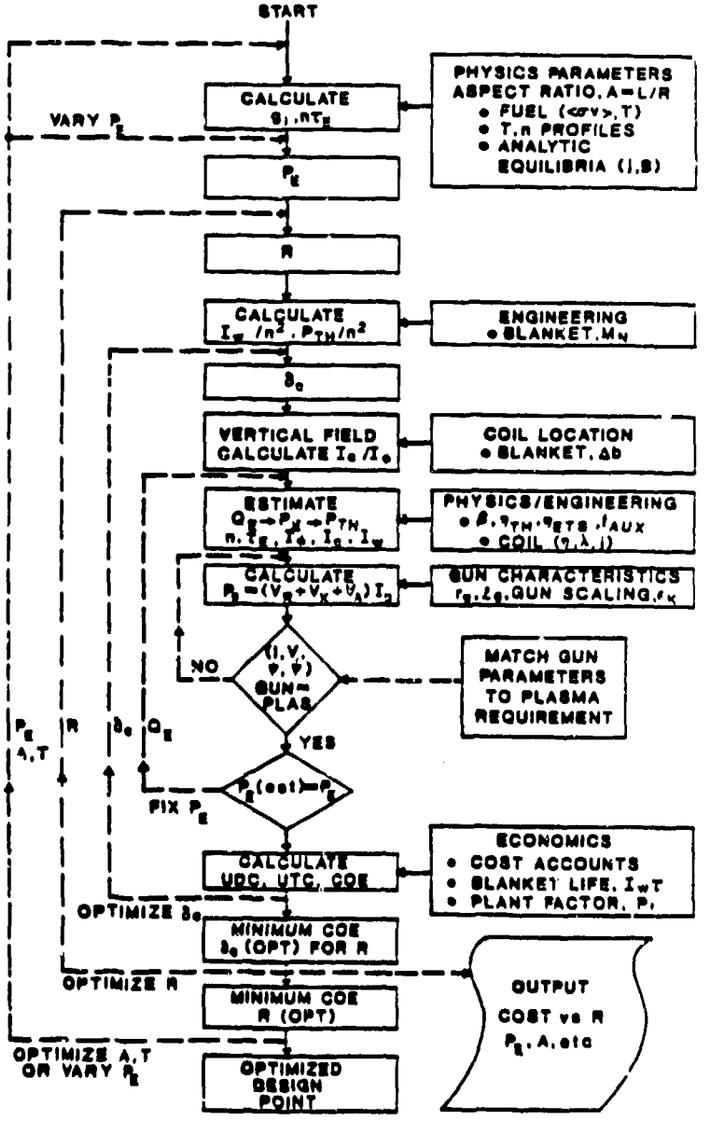

Fig. 3. Logic diagram of spheromak reactor parametric systems model.

Using a first estimate of the system recirculating power, the total thermal power is then determined, and this estimate in turn gives the plasma density and confinement time for a given ignition parameter, $n\tau_E$. Inputing the plasma beta defines all required plasma energies and currents, which then determines the EFC currents. Finally, the total power recirculated to the plasma gun-electrode divertor (hereafter referred to as the "divertor") is determined by the required rate of helicity injection (i.e., resistive decay of plasma currents), ohmic loss in the divertor channel, and electrode arc losses. An iterative loop matches the expected gun characteristics to the spheromak sustainment requirements. An experimentally determined gun scaling that relates geometry, voltage, current, and flux is used[15] to allow a self-consistent analysis. Upon specifying all losses, an updated recirculating power provides a better estimate of the total thermal power, which is iterated according to the algorithm depicted in Fig. 3. until the desired net electric power is achieved; the overall system economic analysis is then performed.

As part of the economic package, the FPC radiation life ($I_w\tau$) couples the neutron first-wall loading, I_w, to the overall plant factor, p_f, and gives a strong COE penalty to high-I_w systems. The costing procedure used in the parametric systems code is an updated version of the Ref. 1. model and reflects the evolution from the original DOE model guidance[16] as driven by recent large reactor studies.[17,18]

B. Plasma Model

A cylindrical equilibrium model[14] is used to determine profile-averaged properties, where generally the pressure is assumed proportional to the square of the poloidal flux. The solution to the force-free equilibrium equation $\mu_0 j = \nabla \times B$, $\mu_0 j = kB$ in cylindrical geometry gives

$$B_r = -B_0 \frac{k_z}{k_r} J_1(k_r r)\cos(k_z z) \qquad (1A)$$

$$B_\phi = B_0[1 + (\frac{k_z}{k_r})^2]^{1/2} J_1(k_r r)\sin(k_z z) \qquad (1B)$$

$$B_z = B_0 J_0(k_r r)\sin(k_z z), \qquad (1C)$$

where $B_\theta = (B_r^2 + B_z^2)^{1/2}$, $k_r = a_{11}/R$, $k_z = \pi/L$, and $k = (k_r^2 + k_z^2)^{1/2}$. The following expression for normalized poloidal flux is used to derive all volume-averaged properties and powers in terms of average density, temperature, and weighting functions, g_i.

$$\psi_{PN}(r,z) = \frac{rJ_1(k_r r)\sin(k_z z)}{(a_{01}/a_{11})\, R\, J_1(a_{01})}, \qquad (2)$$

where $a_{01} = 2.40483$, $a_{11} = 3.83171$, $\psi_{PN}[R_M = (a_{01}/a_{11})R,\ L/2] = 1$, and R_M is the major radius of the magnetic axis. The

calculations depicted on Fig. 3. specify the fusion alpha-particle power and beta, from which the average density results. Pressure balance gives the centerline magnetic field used in Eqs. (1), $B_o^2 = 4\mu_o n k_B T/\beta g_\beta$, where $g_\beta = \langle(\text{mod-}B)^2\rangle/B_o^2$ the volume-averaged beta is β and the plasma toroidal current is $I_\phi = 2B_o k^2[1 - J_o(a_{11})]/\mu_o k_r^2 k_z$. All other plasma quantities can then be derived in terms of the alpha-particle power and β.

It is noted that the coupled physics/engineering/costing algorithm depicted on Fig. 3. yields a plasma confinement time, τ_E(OPT), that is required to assure a minimum-COE design. A separate physics scaling, τ_E(PHYS), must then be compared with τ_E(OPT) to assess the ignition margin available to attain the economic optimum. Such a transport scaling is not yet available for spheromaks, although a scaling of the form $\tau_E(\text{PHYS}) \propto r_p^2 I_\phi^\nu$ is available[1,19] for RFPs, where r_p is the diffusion distance (minor radius in RFPs, $\sim R - R_M \approx 0.372\ R$ for spheromaks) and ν is in the range 1-1.5 for RFPs. Because of the low effective aspect ratios for the spheromak, equilibrium tends to require large I_ϕ compared to an RFP plasma of similar power density; the RFP scaling tends to predict wide ignition margins [i.e., $\tau_E(\text{PHYS}) >> \tau_E(\text{OPT})$] when applied to spheromaks.

C. Fusion-Power-Core (FPC) Model

At the parametrics level of study, FPC detail much beyond that depicted in Fig. 2. is not available, although more detailed conceptual designs on other systems[1,17,18] provide strong guidance. The first-wall heat flux for the spheromak reactor could be low, given effective divertor operation of moderate radiation losses. The blanket/shield stand-off distance, Δb, for resistive copper coil can be in the range 0.6-0.7 m for efficient tritium breeding and heat recovery, although the impact of the blanket displacement by the divertor remains to be estimated.

The EFC thickness and currents are computed by representing both plasma and coils by circular loop conductors ($N_p = 80$, $N_{EFC} = 12$) and solving exactly for the respective inductances. The EFC currents are estimated by requiring the total poloidal flux from both plasma and EFC set to be zero at (R, L/2). Ohmic dissipation in the plasma and EFCs as well as stored energy is computed for use in the energy balance, FPC costing (coil masses, structure, etc.), and ultimately the COE estimate. It is seen from Fig. 3. that an iterative loop on coil thickness determines the cost-optimized EFC parameters as a result of the tradeoff between FPC mass and recirculated power.

D. Electrode-Gun Divertor Model

Along the edge-plasma (open-field) region of the spheromak, the divertor represents the greatest uncertainty for the dc stationary spheromak reactor. The coupled edge-iteratively for the gun voltage, V_g, which along with the gun current, I_g, determines the power that must be recirculated to the dc current drive through the divertor.

The current flowing from the divertor equals the current flowing around the plasma edge on open field lines. Based on Taylor's minimum-energy hypothesis,[12] the ratio of plasma current to field is a constant, $k = \mu_o j/B$, for the $\beta \approx 0$ force-free case considered. If it is assumed that the edge-plasma current density is larger by a factor $1/\varepsilon_K$ than the Taylor current, then $j \approx k B_o/\mu_o \varepsilon_K$, where ε_K is a helicity injection efficiency. Given that a fraction ε of the poloidal flux connects the spheromak with the divertor, then the radius r_o of open poloidal flux at the center of the spheromak is given by $\psi_{PN}(r_o, L/2) = \varepsilon$ and Eq. (2). Hence, $I_g = \pi r_o^2 k B_o/\mu_o \varepsilon_K$.

Given the gun voltage, $V_g = V_{gK} + V_{gR} + V_{gA}$, the power to the gun, $P_g = V_g I_g$, can be determined, the total recirculating power results, and the optimization proceeds as depicted on Fig. 3. The electrode arc voltage drop, V_{gA}, is varied as parametric input, whereas a one-dimensional parallel-field heat-conduction model estimates the temperature profile around the open field lines for an assumed electrode-plasma temperature, T_{EL}. The voltage V_{gK} needed to supply magnetic helicity at a rate $2V_{gK}\varepsilon\psi$ equal to the resistive decay, K/τ_{B2}, is determined from the plasma field diffusion time, τ_{B2} = (field energy)/(ohmic power), these latter quantities being determined from the equilibrium model [Eqs. (1)] or more exact solutions[1] to the MHD equilibrium equations for the Taylor state. Hence, the component of the gun voltage needed to drive helicity is $V_{gK} = K/2\varepsilon\psi\tau_{B2}$, where $\tau_{B2} \approx (A_p^2/V_p)L_p/2g_{OHM}\eta$, $A_p \approx RL$, $V_p = \pi R^2 L$, L_p is the plasma internal inductance, g_{OHM} is the ohmic-heating profile factor, and η is the plasma resistivity evaluated at the average plasma temperature. For the model equilibrium, $\psi = 2\pi a_{01} J_1(a_{01}) B_o/k_r^2$, $K \approx 1.07\psi\phi$, and the toroidal flux is $\phi = (2k/k_r^2 k_z)[1 - J_o(a_{11})]B_o$. Given an experimentally determined relation between r_o, ε, V_g, and the gun dimensions (e.g., inner and outer electrode radii, r_{gi}, and r_{go}), a self-consistent set of plasma/gun-electrode/divertor equations results. A plasma-gun scaling has been suggested for the CTX experiment[14] and is used in this study.

$$I_g/V_g^{1/3} \approx 6(10)^3\,[1.0 + 10^3\varepsilon\psi(0.15/r_{go})] \qquad (3)$$

Lastly, specification of a design heat flux, q_D(MW/m^2), and a heat/particle (i.e., magnetic flux) distribution along the divertor axis, as well as an estimation of the power split of plasma energy loss between inner and

divertor length, ℓ_g (Fig. 2.). These relations together with the optimization logic depicted on Fig. 3. give a tightly focused reactor model with which to select a well constrained set of spheromak design points.

IV. PARAMETRIC RESULTS AND SAMPLE DESIGN POINT

A. Standard Conditions

Table I lists the "standard" conditions adopted for this study. Sensitivity studies were performed about these standard conditions.

TABLE I
Standard Conditions for Spheromak Reactor Study

Density and temperature profiles, $n(r,z)$ and $T(r,z)$	$\Phi_{PN}(r,z)$
Plasma impurity level, Z_{EFF}	1
Spheromak aspect ratio, L/R	1.25
Taylor parameter, $k(m^{-1}) = \mu_o \vec{j}/\vec{B}$	CONSTANT
Volume-averaged beta, β	0.1
Average plasma temperature, T(keV)	20
Edge-plasma temperature, T_E(keV)	0.5
Electrode-plasma temperature, T_{EL}(eV)	3.0
Helicity injection efficiency, ε_K	0.66
Electrode arc voltage, V_{gA}(V)	0.0
Plasma gun scaling	[Eq. (3)]
Ignition parameter, $n\tau_E(10^{20}s/m^3)$	$f(g_i,T)$
Divertor design heat load, $q_D(MW/m^2)$	5.0
Blanket/shield thickness, Δb(m)	0.7
Blanket energy multiplication, M_N	1.3
Gun electrode radius radio, r_{gi}/r_{go}	2/3
FPC radiation life, L_w(MWyr/m^2)	15.0
Scheduled FPC change-out time (days)	28.0
Thermal conversion efficiency, η_{TH}	0.35
Auxiliary power fraction, f_{AUX}	0.07

B. Parametric Results

The minimum-COE designs are shown on Fig. 4. as a function of outer plasma radius, R(m), and net-electric power, P_E(MWe), for the standard conditions. Lines of constant neutron first-wall loading are also shown, indicating that the fully optimized minimum-COE design occurs near $I_w \approx 20$ MW/m^2 for the 15 MWyr/m^2 FPC life assumed. The nuclear economy-of-scale that characterizes the costing data base and procedure used[1,17,18] substantially reduce the COE as P_E is increased from 250 to 1000 MWe(net).

Large plasma radii force low neutron first-wall loadings, larger FPC mass, and the observed increase in COE. Because FPC mass utilization is even smaller than that projected for the CRFPR,[1] the fraction of the total direct cost represented by the FPC is even less (3-4%), and an even weaker increase in COE with increased plasma size is observed. Substantial decreases from the first-wall neutron loading of $I_w \approx 20$ MW/m^2 for the fully optimized minimum-COE design would be possible without serious cost penalty, although the plasma size for $I_w < 10$ MW/m^2 and $P_E > 500$ MWe large. The low cost of the FPC, however, should allow an economical multiplexing of a number of smaller, lower-wall-loading FPCs to drive a ~ 1000-MWe plant.

As the plasma radius and size is diminished, Fig. 4. shows a rapid increase in neutron first-wall loading for a given P_E. The increased downtime required for the more frequent FPC replacement rapidly drives the COE upward. Decreases in the FPC radiation life or increases in the FPC maintenance period will cause this minimum-COE point to occur at lower I_w values. Counteracting this tendency for increased COE as I_w increases for a given P_E is a coupling of plasma and coil currents that does not deteriorate as rapidly as for the CRFPR case, leading to a less rapid decrease in recirculating power as R is decreased. The upswing in COE depicted in Fig. 4, therefore, is not as strong as projected for the CRFPR.[1]

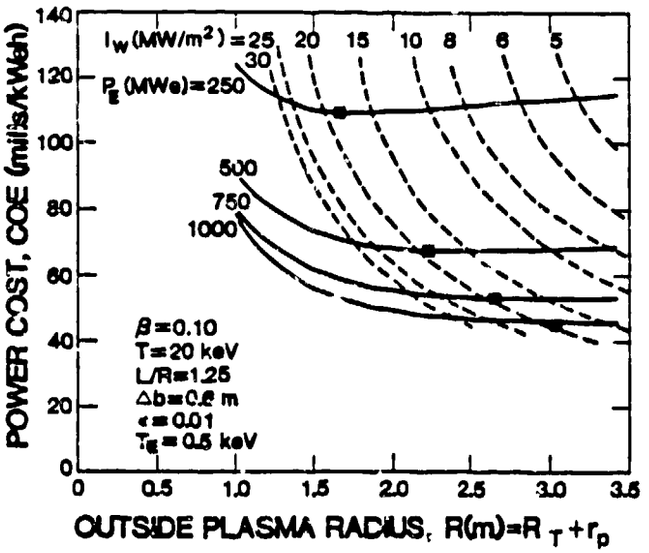

Fig. 4. Cost of electricity as a function of plasma dimension and net electric power.

C. Sample Design Points

Table II summarizes key plasma and FPC parameter for the fully optimized minimum-COE design points over a range of P_E(MWe). The total power required by the gun is expressed as a plasma Q-value, $Q_p = P_F/P_g$, in Table II, where $P_F = P_{TH}(4M_N + 1)/5$ is the fusion power. Because of the low aspect ratio, equilibrium requires substantially higher values of plasma currents than for the RFP,[1] although the larger plasma minor cross sections for the spheromak result in a decrease in plasma current density. The near-spherical geometry also is reflected in: a) reduced FPC power density, but b) decreased FPC mass utilization and a greater reduction in the impact of the FPC on the total direct cost. Because almost all the alpha-particle and ohmic dissipation within the plasma is assumed to be transported

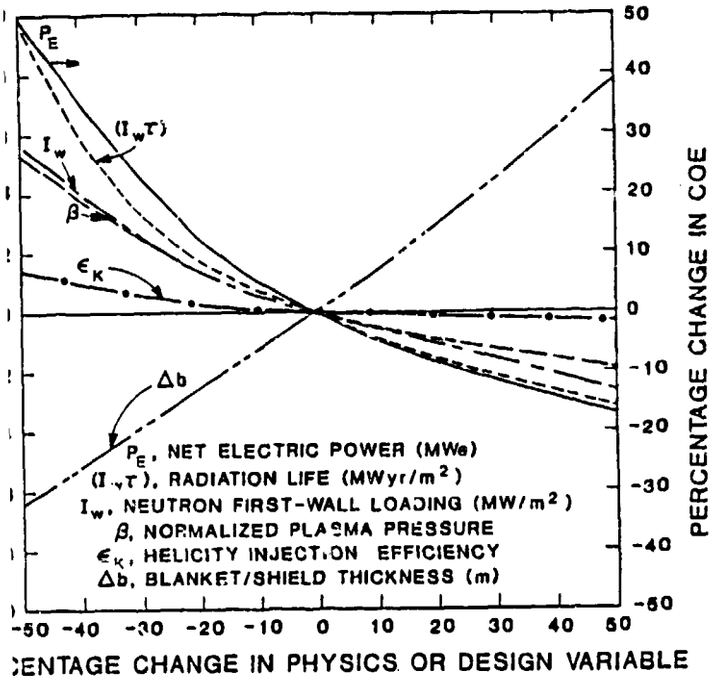

g. 5. Sensitivity of cost of electricity to key physics and engineering parameters.

heat flux limitation imposed results in the divertor being a large fraction of the FPC volume (Table II).

D. Sensitivity Studies

Seven key variables were identified for sensitivity analyses: helicity injection efficiencies, ϵ_K; volume-average plasma beta, β; edge-plasma temperature, T_E; fusion-neutron first-wall loading, I_w, blanket/shield thickness, Δb; FPC radiation life, $I_w\tau$; and arc voltage drop at the electrode-gun divertor, V_A. Figure 5 summarizes the COE sensitivity to the net electric power, P_E, and most of the above-mentioned variables. Over the range of P_E studied (500-1500 MWe), the ohmic losses in the plasma do not dominate the recirculating power, giving a weak dependence of COE on ϵ_K and T_E, (the T_E dependence is not shown, but is < 1%). Increases in V_A generally caused the minimum-COE designs to select a larger value of total gun voltage, V_g, in order to minimize gun current and associated arc losses, thereby giving a weaker dependence of COE on V_g than originally expected (the V_g dependence is also < 1% and is not shown on Fig. 5.)

V. CONCLUSIONS

The spherical-like reactor geometry presents both advantages and disadvantages. Because of the higher ratio of volume to surface, better (lower) FPC mass utilization occurs for a lower FPC power density, but the

TABLE II

Fully Optimized, Minimum-COE Spheromak FPC Design-Point Summary (Fig. 4)

Net electric power, P_E(MWe)	250.	500.	750.	1000.
Thermal power, P_{TH}(MWt)	973.	1803.	2605.	3416.
Spheromak radius, R(m)	1.70	2.22	2.60	3.00
Spheromak height, L(m)	2.12	2.77	3.25	3.72
Spheromak volume, $V_p = \pi R^2 L$(m^3)	18.34	42.89	69.02	105.18
Plasma current, I_ϕ(MA)	30.0	37.5	42.7	47.3
Plasma current density, j_ϕ(MA/m^2)	8.3	6.1	5.1	4.3
Average plasma density, n(10^{20}/m^3)	2.8	2.5	2.4	2.3
Average plasma temperature, T(keV)	20.	20.	20.	20.
Optimum energy confinement time, τ_E(OPT)(s)	0.34	0.38	0.40	0.43
Peak field on plasma centerline, B_o(T)	13.9	13.3	12.9	12.5
Plasma field, B(R,L/2)(T)	5.6	5.4	5.2	5.0
EFC field, B_c(T)	3.0	2.8	2.7	2.6
Total field energy, W_B(MJ)	343.5	701.1	1065.3	1494.4
Field decay time, τ_B2(s)	25.7	44.0	60.0	78.6
Plasma ohmic dissipation, P_Ω(MW)	13.4	16.0	17.8	19.0
Plasma fusion power density, P_F/V_p(MW/m^3)	42.2	33.6	30.2	26.0
Fusion neutron first-wall loading, I_w(MW/m^2)	17.4	18.7	19.8	19.8
Total thermal power, P_{TH}(MWt)	973.	1803.	2605.	3416.
Mass utilization, M_{FPC}/P_{TH}(tonne/MWt)	0.41	0.29	0.26	0.24
FPC power density, P_{TH}/V_{FPC}(MWt/m^3)	8.69	10.20	10.59	10.65
FPC dimensions				
• First-wall radius, r_w	1.70	2.22	2.60	3.00
• EFC thickness, δ_c(m)	0.59	0.56	0.59	0.57
• Inner electrode radius, r_{gi}(m)	0.95	1.24	1.45	1.66
• Outer electrode radius, r_{go}(m)	1.42	1.86	2.17	2.49
• Electrode length, ℓ_g(m)	2.29	3.13	3.85	4.38
• System radius, r_s(m)	2.99	3.48	3.88	4.25
• Mass (tonne)	395.	524.	685.	806.
• Gun-electrode volume fraction	0.12	0.16	0.19	0.21
Plasma Q-values, $Q_p = P_F/P_\Omega$	37.	60.	76.	94.
Recirculating power fraction	0.27	0.21	0.18	0.16
Unit direct cost, UDC($/kWe)	2441.9	1480.9	1147.4	977.7
Cost of electricity, COE(mills/kWe)	109.4			

combination of high power density and high total power can be achieved only for higher first-wall neutron loadings. Equilibrium in a low-aspect-ratio, spherical-like geometry also requires large plasma currents, but both the plasma current density (and ohmic heating rates) as well as stored energy remain low.

The physics issues and the impact on reactor performance can be divided between the spheromak and the divertor. The sustained spheromak may require a constant $k = \mu_0 j/B$ profile, inferring that large Taylor currents must flow in the cold plasma edge. High edge-plasma temperatures are needed to minimize joule losses incurred therein, which in turn can impact the power consumed by the divertor.

The divertor appears to be a key system in determining the viability of this concept as a steady-state, stationary reactor. The exo-reactor location of the divertor gives greater design and maintenance flexibility to this high-heat-flux unit. The impact of the divertor on blanket efficiency remains to be quantified. The gun scaling relationship [Eq. (3)] represents a large uncertainty and determines the fraction of poloidal flux diverted, which should remain below ~ 0.01 in order to minimize power requirements. Lastly, the plasma processes active in the transition region between the divertor and the spheromak involve magnetic helicity generation, transport, and absorption, and. therefore, are characterized by related unknowns.

The results presented herein appear promising from the viewpoint of simplified FPC, smaller nuclear system, and the possibility to shrink the nuclear envelope to an extent where fusion assumes an economy of scale that is more like fossil-fuel systems. In this case, smaller power plants would become more attractive economically, multiplexing a number of small low-cost FPCs to drive a large total plant may be possible, and off-site factory construction of a greater part of the nuclear system may be possible.

ACKNOWLEDGMENTS

The authors express their gratitude to Tom Jarboe and Cris Barnes of Los Alamos for many enlightening discussions.

REFERENCES

1. R. L. HAGENSON, et al., "Compact Reversed-Field Pinch Reactors (CRFPR): Preliminary Engineering Considerations," Los Alamos National Laboratory report LA-10200-MS (August 1984).

2. T. R. JARBOE, et al., Phys. Rev. Lett. 45, 1264 (1980).

3. W. C. TURNER, et al., J. Appl. Phys. 52, 175 (1981).

4. G. C. GOLDENBAUM, et al., Phys. Rev. Lett. 44, 393 (1980).

5. M. YAMADA, Phys. Rev. Lett. 46, 118 (1981).

6. M. KATSURAI and M. YAMADA, Nucl. Fus. 22 (11), 1407 (1982).

7. A. M. M. TODD, et al., Proc. 15th Intersoc. Energy Conversion Engineering Conference 3, 2229 (August 18-22, 1980).

8. A. C. SMITH, JR., et al., Proc. 9th Inter. Conf. on Plasma Physics and Controlled Nuclear Fusion Research (Paper IAEA-CN-41/O-2-2) (September 1-8, 1982).

9. A. MOHRI, et al., "Conceptual Design of a Moving Ring Reactor, KARIN-I," Proc. 6th Topical Meeting on the Technol. of Fusion Energy, San Francisco, CA (March 3-4, 1985).

10. T. R. JARBOE, et al., Phys. Rev. Lett. 51, 39 (1983).

11. T. R. JARBOE, Proc. 5th Symp. on Physics and Technology of Compact Toroids in Magnetic Fusion Energy Program, Bellevue, WA (November 16-18, 1982).

12. J. B. TAYLOR, Phys. Rev. Lett. 33, 1139-1141 (1974).

13. T. R. JARBOE, et al., 10th Inter. Conf. on Plasma Phys. and Controlled Nucl. Fus. Res., London, UK (1984).

14. J. M. FINN, et al., Phys. Fluids 24, 1336 (1981).

15. C. BARNER and T. R. JARBOE, personal communication, Los Alamos National Laboratory (1984).

16. S. C. SHULTE, et al., Pacific Northwest Laboratory report PNL-2987 (September 1979).

17. C. C. BAKER (Principal Investigator), et al., "STARFIRE - A Commercial Tokamak Fusion Power Plant Study," Argonne National Laboratory report ANL/FPP-80-1 (September 1980).

18. D. E. BALDWIN, et al., MARS Mirror Advanced Reactor Study," Lawrence Livermore National Laboratory report UCRL-53480 (July 1984).

19. R. S. MASSEY, Proc. 6th ANS Topical Meeting on Technol. of Fusion Energy (March 3-7, 1985).